Published in final edited form as:
Chem Mater. 2010 ; 22(9): 2814–2821. doi:10.1021/cm903740e.

CdSe Quantum Rod Formation Aided By In Situ TOPO Oxidation

Abraham Wolcott[‡], **Robert Carl Fitzmorris**[‡], **Omed Muzaffery**[‡], and **Jin Z. Zhang**[‡,*]
[‡]Department of Chemistry and Biochemistry, University of California, Santa Cruz, CA 95064 USA

Abstract

In-situ TOPO decomposition was accomplished by applying a vacuum at elevated temperatures to a precursor solution in the presence of oxygen, leading TOPO to oxidize to di-n-octylphosphinic acid (DOPA) and octylphosphonic acid (OPA). The mixed ligand system of tetradecylphosphonic acid (TDPA), DOPA and OPA produced CdSe QRs on the order of 4 nm in diameter and 20 nm in length. Solvent and ligand identification was performed by mass spectrometry and ^{31}P nuclear magnetic resonance spectroscopy. Transmission electron microscopy (TEM) was utilized to determine the morphology, size and crystal growth of the CdSe QRs. This method of CdSe QR synthesis is unique in that the phosphonic acids responsible for anisotropic growth are formed in situ, prior to the nucleation and growth of the nanorods. Without the oxidation of TOPO, CdSe quantum dots (QDs) were synthesized instead, as reported previously. This discovery reinforces the efficacy of DOPA and OPA molecules as critical ligands in the formation of 1-dimensional (1D) nanostructures.

Introduction

Semiconductor nanoparticles (NPs), nanorods (NRs) and heterostructures have been widely studied for their unique electronic, photophysical, and transport properties, as well as for their use in devices.[1-14] Advancements in wet chemical synthesis techniques have lead to homogenous size distributions, high quantum yields and safer precursor materials. Growth mechanisms of CdSe nanorods and CdTe tetrapods have been explained by the preferential attachment of ligands to certain crystal facets, precursor concentration levels and temperature dependent crystal phase growth.[8, 11] Anisotropic growth of unique crystal facets leads to 1D nanostructures of varying diameter and length. Nanomaterials spanning a broad range of dimensions and sizes have been fervently examined over the past decade. Their unique optical properties inherent in quantum confined systems have lent these materials to be utilized in biological labeling, optoelectronics, and photovoltaic cells.[15-22] High degrees of synthetic control are necessary for both fundamental and device investigations, but the mechanisms of nanocrystal growth are not completely understood.

Currently, the understanding of crystal growth mechanisms of nanomaterials can be broken down into four parts: (1) initial nucleation based on critical concentration precipitation, (2) monomer diffusion and addition to nucleated sites, (3) ligand preferential binding characteristics, and (4) inherent crystal facet potential energy.[23-26] A recent in-situ TEM study also points to NP-NP coalescence as a driving force in NP growth kinetics.[27] Nanocrystal nucleation is typically understood as a supersaturation of precursor material in solution leading to an arrested precipitation state meditated by surfactants. This has been accomplished by the quick injection of precursor materials into aqueous or organic solvents. Subsequent heating then facilitates growth by the addition of solubilized monomers that can then add to the

*Corresponding Author: zhang@chemistry.ucsc.edu.

Supporting Information Available. Additional TEM images of CdSe QDs/bipods/tripods/tetrapods, MS, and NMR spectra of control solutions. This material is available free of charge at via the Internet at http://pubs.acs.org.

nucleated cluster. Small clusters or "magic" size assemblies of II-VI semiconductors have been reported and their photophysical properties investigated.[28-31] These ultra-small clusters are recognized by even further blue shifted absorption and emission characteristics from their larger nanoparticle counterparts.

In going from zero dimensional (0D) QDs to 1D QRs, ligand composition and monomer concentration have been found to be critically important experimentally. An initial report on nanorod synthesis in 1999 included the use of only technical grade TOPO, and quickly injected Cd and Se precursors dissolved in tributylphosphine.32 While the CdSe QRs were only 8 nm × 13 nm, it became apparent that anisotropic growth could be accomplished with the organometallic route as it had been with studies utilizing the vapor-liquid-solid (VLS) methods.[33] Impurities in the technical grade TOPO were the likely culprit in the formation of anisotropic 1D nanostructures. Technical grade TOPO at 90 % purity was known to possibly include degraded phosphonic acids produced during synthesis due to side reactions. Various "batches" with different lengths of aging were discovered to produce either QDs or QRs with the same synthetic protocol. Later on, controlled CdSe QR growth was accomplished with the use of high purity TOPO, hexylphosphonic acid (HPA) or tetradecylphosphonic acid (TDPA).[8, 34, 35] High aspect ratios could then be more reproducibly achieved due to the precise control over the chemical composition of the reaction solution. Synthetic impurities from technical grade TOPO were usually not considered as a hindrance to the full control over the ligands, the phosphonic acids, which effectively control the nanocrystal growth. On the contrary, it has been noted recently that even in 99% TOPO 10 synthetic impurities have been identified, as will be discussed in more detail later.[36]

A number of theoretical studies have delved into the role of surfactants and their binding affinity to three major crystal facets of CdSe.[26, 37-40] Ab initio calculations performed by Puzder *et al*. utilized density functional theory (DFT) on $Cd_{15}Se_{15}$ and $Cd_{33}Se_{33}$ clusters to understand the dynamics of QD and QR growth.[37] In their study they attached four ligands; phosphine oxide, phosphonic acid, carboxylic acid and trimethylamine to the polar and apolar facets of wurtzite CdSe. The polar facets of 0001 and $000\bar{1}$ are the growth directions responsible for the anisotropic growth of CdSe QR (ends), while $01\bar{1}0$ and $11\bar{2}0$ are the apolar facets that represent the sides of an individual QR. Consequently the *ab initio* calculations showed that the binding energies of phosphine oxide and phosphonic acid were appreciably stronger on the apolar facets (~1.23-1.45 eV) compared to the less stable polar facets (~0.63-1.11 eV). Binding was generally dominated by surfactant-Cd interactions, and it was found that surfactant molecules placed next to surface apolar Se atoms would quickly find their lowest energy state bound to a Cd site. The weaker binding affinity to the polar facets in turn means that the removal of that surfactant molecule will be easier, and addition of Cd and Se monomers will be accelerated.[26] Increased crystal facet growth velocities leads to the anistropic growth inherent in CdSe QRs along the weakly bound 001 growth directions. Interestingly, along the 0001Cd facet it was found that 100% surfactant coverage would lead to a thermodynamically favorable removal of a surfactant molecule due to increased electron density on that facet.26 These thermodynamic considerations reinforce how subtle changes in reaction conditions such as TOPO impurities can have drastic results on morphology.

TOPO has been the central solvent in the organometallic route for II-VI semiconductors and has revolutionized the standards for size dispersity, crystallinity, quantum efficiency and morphology of quantum confined nanomaterials.[8, 23, 24, 32, 41, 42] Recently, several studies have used NMR and MS analysis to precisely investigate the composition of TOPO/phosphinic/phosphonic acid based CdSe nanocrystal synthesis.[36, 43-45] While it has been nearly a decade since the initial investigations of the connection between morphological control and impurities in technical grade TOPO began, only recently have some of the details began to emerge.[46] Wang *et al*. identified 10 common impurities found in 90% TOPO and 99% TOPO batches.

Through thorough examination, they made the case that the relative ratio of impurities in various batches of TOPO (tech and high purity) either hinders, allows for, or has no effect on the synthesis of high quality CdSe nanowires.[36, 44] Of the impurities they highlighted, DOPA and di-n-octylphosphinic acid were recognized as a key component in the successful growth of high quality CdSe nanowires. Wang *et al*. justified DOPA's efficacy in CdSe growth by explaining that DOPA modifies the formation of CdSe through the ligand substitution of precursor materials. To test their theory, they added successive amounts of DOPA, OPA and mono-noctylphosphinic acid (MOPA) to examine the resulting quality of their CdSe nanowires. Additions of DOPA, OPA and MOPA to medium and poor quality TOPO batches subsequently resulted in high quality CdSe nanowire formation. Batches of commercially available TOPO that resulted in superior CdSe nanowire formation were understood to have beneficial amounts of DOPA.

In the present work, we reinforce that DOPA and OPA are also critical to the growth of much smaller, 4 nm × 20 nm CdSe QRs. In a deviation of Wang's work, we have identified that DOPA and OPA were produced when residual oxygen was allowed to persist in the reaction solution of CdO/TOPO/TDPA under a weak vacuum of 1000 mtorr, and a vacuum was applied at elevated temperatures of ~280-300 °C. In-Situ DOPA and OPA formation via TOPO oxidation were apparent due to a change in coloration of the solution and smoke formation, understood to be 1-octene degradation. The CdSe QRs and their precursor solutions were characterized with optical spectroscopy, electron microscopy, mass spectroscopy (MS), and nuclear magnetic resonance (NMR) spectroscopy.

Experimental Section

The CdSe QRs studied here were synthesized via a modified organometallic method in a coordinating solvent of TOPO and TDPA based on the work of Peng *et al*.[34, 35, 47] The CdSe QRs were produced in common "air-free" conditions on a nitrogen filled Schlenk line. Briefly, 50 mg CdO (Acros Organics #22379, 99%), 4.1 g of TOPO (Strem Chemicals #15-6661, 99%) and 305 mg TDPA (PCI synthesis # 4671-75-4, 99%) were placed in a 50 mL three neck flask with septa, thermocouple and refluxing column attached to the Schlenk line. In order to remove residual water and some oxygen from the mixture, the solution was heated to 120 °C under nitrogen flow and subsequently placed under a weak vacuum. During the degassing process, the vacuum was held at 1000 mtorr or higher. This was done to insure dissolved oxygen was significant enough to oxidize TOPO in an observable amount. A 0.16 M SeTOP solution was prepared in a nitrogen filled glovebox by placing 4 mL of technical grade tri-n-octylphosphine (Aldrich #117854, 90%) and 42.0 mg Se powder (Acros Organics #19807, 99% 200 mesh) into a scintillation vial, capped with a septum and stirred vigorously. After removal from the glovebox, the SeTOP solution was sonicated for 30-45 seconds to insure complete dissolution of the Se powder. The SeTOP solution was optically clear, colorless and had no visible Se particles. After three nitrogen purge and vacuum cycles (≥1000 mtorr), the solution of CdO in TOPO/TDPA was optically clear with no color→ slight golden tint by 250 °C. Special care was taken that all CdO was completely dissolved and no residual CdO powder resided on the flask walls by vigorously shaking the vessel. At ~ 280-300 °C, the nitrogen flow was ceased and a weak vacuum was applied to the CdO/TOPO/TDPA solution. A smoke formed above the solution, the solution color changed to a darker golden hue, the vacuum was stopped and a nitrogen flow was applied. Aliquots of the pre and post-oxidation steps were collected for MS and NMR analysis. With a solution temperature of 270 °C, 4.0 mL of the 0.16 M SeTOP was injected, and upon injection the temperature decreased to 230 °C. The injection needle was purged of oxygen prior to SeTOP addition by placing the syringe into the Teflon capped vial of SeTOP with a constant flow of nitrogen. Growth of the CdSe QRs was performed at 260 °C, and tracked via UV-Vis spectroscopy and photoluminescence (PL) spectroscopy by extracting small aliquots from the reaction mixture into toluene. Growth was allowed to

continue for 20 minutes, then allowed to cool to approximately 50 °C, 7 mL of toluene was injected and then the QRs were precipitated with 5-10 mL of methanol. Three precipitation and decantation cycles were performed by dispersing the QRs in toluene and precipitating with methanol. The CdSe QRs were ultimately left as a solid and then dissolved in toluene or chloroform as needed.

All UV-visible (UV-vis) absorption spectra were performed on a Hewlett Packard 8452A diode array spectrophotometer (Palo Alto, CA). Photoluminescence (PL) spectroscopy was measured on a Perkin Elmer LS 50B (Fremont, CA) with an excitation wavelength of 390 nm and 1% attenuator. Samples were placed in open sided 1 cm path length quartz cuvettes for both PL and UV-Vis measurements. PL measurements were made with CdSe QR concentrations between 0.1-0.3 absorption units at 390 nm, and no normalization was used. Transmission electron microscopy (TEM) was carried out on a JOEL 1200 EX with a Gatan CCD and software. TEM and high resolution TEM images were obtained with a Phillips CM200/FEG (Field Emission Gun) microscope at the National Center for Electron Microscopy (NCEM) at Lawrence Berkeley National Laboratory in Berkeley, CA. ^{1}H and ^{31}P nuclear magnetic resonance (NMR) was carried out on samples dissolved in deuterated chloroform and experimentation was performed on a Varian Unity 500. Mass Spectroscopy (MS) was conducted by dissolving small amounts of the pre and post combustion CdO/TOPO/TDPA solutions in methanol (ng/L) and data was collected on a Thermo Finnigan LTQ (San Jose, CA,). The MS had an electron spray injection with a capillary temperature of 275 °C, a positive polarity of +4.5 kV and a negative polarity of −5.00 kV.

Results

CdSe Quantum Dot vs. Quantum Rod Growth

Under normal reaction conditions without TOPO oxidation, CdSe QD formation would dominate as seen by Peng using CdO as a precursor.[47] If QD formation proceeded due to a failed TOPO oxidation, two distinct characteristics would prevail; (1) no smoking or change in coloration would be present to the precursor solution, and (2) the growth of the QD diameter would happen on faster time scales in comparison to QR formation. During the growth of either CdSe QDs or QRs, aliquots of the growth solution were dissolved in toluene, and utilized to track the nanocrystal growth via UV-vis absorption spectroscopy. First excitonic peak positions during a QD synthesis would take ~5 minutes to reach 575 nm. In contrast, during QR synthesis it would take a 20 minute growth period to evolve a first exciton peak to 575 nm. The bulk room temperature linear absorption and PL spectra of the CdSe QRs are shown in Figure 1. The first excitonic peak for quantum confined CdSe first appeared around 500 nm and continued to red shift until ca. 575-580 nm in the UV-Vis spectra. Red-shifting of the excitonic peak is representative of the quantum confined CdSe QR diameter, and is not defined by the length of the QR. This continuous shifting is indicative of the dynamic increase of the QR diameter during the growth period at 260 °C. Therefore, Cd and Se monomers are being added to both the unique c-axis facet (polar facets 0001 and $000\bar{1}$), and the facets representative of the QR diameter simultaneously (apolar $01\bar{1}0$ and $11\bar{2}0$ facets). As supported by Puzder and Manna, the phosphonic acids are more weakly bound to the polar facets, causing surfactant removal to happen more readily from the polar facet, thus allowing for faster addition of Cd and Se precursors.[26, 37] Subsequently, the more tightly bound apolar facets passivated by phosphonic acids are still displaced due to the high temperature of the growth solution (260 °C), but allow for Cd and Se addition at a reduced rate. Similarly, the PL spectra displayed a red-shift in band-edge luminescence as the QRs were growing, and there were no indication of shallow/deep trap state emission. Raw QRs did display a blue shifted emission shoulder (in relation to band-edge peak) prior to solution precipitation and resuspension (data not shown). The PL shoulder was understood to be emanating from spherical QDs in the ensemble that

were later separated by the cleaning process. For the final QRs, the peak of the PL is Stokes-shifted from the absorption by approximately 7 nm from 575 nm to 582 nm and the PL band has a full-width at half-maximum (FWHM) of 35 nm. From the bulk absorption and PL measurements, an effective CdSe diameter of approximately 4 nm can be inferred.[48]

TEM images showed that the phosphonic acid capped CdSe QRs were ca. 4 nm × 20 nm, in good agreement with particle diameter as a function of excitonic peak position (Figure 2A). While most of the CdSe QRs have an aspect ratio of 5:1, other nanostructures were also observed, including bipods, tripods and tetrapods that account for <5% of the products (Supporting Online Material (SOM)/S1). The observation of bipods, tripods and tetrapods was first reported on by Manna *et al*., and later investigated thoroughly in the case of CdTe tetrapods.[8, 11] Branching was observed in the ensemble of CdSe QRs, and is believed to be due to the nature of the mixed ligand system and the varying alkyl chain length used to grow the CdSe QRs. A systematic study of CdSe QR growth as a function of varying the phosphonic acid alkyl chain length (6-18 carbon) reported branching percentages ranging from 0% with noctadecylphosphonic acid to > 99% when using hexylphosphonic acid.[49] Our surfactant system contains both 8 and 14 carbon chain phosphonic acids, leading to a moderate amount of branching (~25%). In our case, the mixed ligand system produces non-uniform steric hindrance at the nanocrystal surface, as multiple molecular species compete for polar and apolar binding sites. Increased hydrophobic interactions from bound surfactant molecules to apolar facets should provide additional stabilization along the sides of the QR, thus reducing branching. While theoretical studies show only minor binding energy changes (0.01 eV) between methyl and full chain phosphine oxides and phosphonic acids, experimental results show markedly different results.[37, 49] Both steric affects and hydrophobic interactions may play some role in these discrepancies. HRTEM imaging reveals the lattice fringes of single crystalline CdSe QRs, and a lattice constant of ~3.6 Å was measured along the long axis of the individual QR (Figure 2B). The lattice spacing of 3.57 Å is representative of the 001 crystal facet of wurtzite CdSe and is consistent with previous reports.[50] Dislocations and vacancies can also be seen in the HRTEM images of some of the representative CdSe QRs.

Identification of DOPA and OPA as the Main Products of TOPO Oxidation Following Smoking

In a typical synthesis of CdSe QDs, the three basic precursors, CdO, TOPO and TDPA are used in conjunction with a selenium trioctylphosphine (SeTOP) or selenium tributylphosphine (SeTBP) solution. By modifying the relative concentration of TDPA the controllable synthesis of QRs can be attained.[34, 35] Prior to SeTOP or SeTBP injection, the precursor solution would typically be thoroughly degassed to remove bound water and oxygen. In our case, we allowed a weak vacuum of 1000 mtorr at 120-150 °C to take place during the degassing step. Due to the relatively weak vacuum, adsorbed oxygen remains present in the CdO/TOPO/TDPA solution. At elevated temperatures of 280-300 °C and in conjunction with an applied vacuum, resulted in a smoking of the solution, and a modification of the coloration of the solution from colorless→light golden hue or light golden hue→darkened golden hue. This general change in the coloration was an obvious indicator of a chemical transformation taking place. During the oxidation of TOPO, four molecular species were produced; (1) DOPA, (2) 1-octene, (3) OPA and (4) mono-n-octylphosphinic acid (MOPA). We believe the combustion of 1-octene is responsible for the smoking that was observed. Since the oxidation of TOPO was performed at 280-300 °C, the evolution of 1-octene is above the autoignition temperature of 230 °C, and was found to decompose rapidly. Initially, poorly controlled reactions of TOPO oxidation led to minor flames at the surface of the CdO/TOPO/TDPA during the applied vacuum, and were extinguished when the vacuum was ceased. MS and NMR spectra of pre-oxidation and post-oxidation solutions were the general tool used to determine their molecular composition. Consequently, 1-octene was not readily identified using either experimental technique.

MS data of an aliquot of the pre-oxidation CdO/TOPO/TDPA solution in negative mode shows two major peaks (Figure 3A). The main peak is representative of TDPA at 277.25 mass/charge units and the second largest is at 289.27 representative of the molecule DOPA, and was mentioned previously as the major impurity in both tech and 99% TOPO batches.[36, 44] The relative abundance of TDPA was considered 100%, while DOPA's relative abundance in comparison was at 14%. The presence of DOPA prior to oxidation was reinforced by control TOPO samples that revealed the largest impurity to be DOPA (SOM/S2). The control TDPA MS data shows no other peaks than those representative of TDPA, and therefore we can conclude that any additional peaks prior to oxidation are caused by TOPO impurities (SOM/S3). In the original pre-oxidation solution, OPA was detected at a relative abundance of 0.75%, and could have been formed from minor TOPO oxidation at elevated temperatures. The drastic increase in relative OPA and DOPA concentration is evident after the combustion step is applied.

Post-oxidation MS data shows not only TDPA and DOPA peaks, but also the appearance of the OPA molecule produced during the oxidation step of the synthesis and a change in the relative abundance ratio of TDPA/DOPA (Figure 3B). Pre-oxidation data confirms that OPA was not significantly present (0.75%) in the Cd/TOPO/TDPA mixture, but was instead chemically produced at high temperature (280-300 °C), with residual oxygen and an applied vacuum. If during the initial degassing portion of the synthesis, the overall pressure became lower than ~1 torr (120-150 °C), we would not observe any smoking of the solution, and the color of the solution would be unchanged and the MS spectra would not show representative peaks of OPA (SOM/S4). In turn, the synthesis would produce CdSe QDs instead of QRs consequently, as seen by TEM studies (SOM/S5). Post-oxidation MS data also shows no indication of 1-octene being present at ~ 112 mass/charge units. Since the generation and rapid decomposition of 1-octene above its autoignition temperature was instantaneous, no dissolved 1-octene was evident in the aliquots. Another important observation is the drastic increase in the DOPA relative abundance in comparison to that of TDPA as mentioned previously. Originally a relative abundance of TDPA:DOPA was 1:0.14, but after the combustion step we see that altered significantly to a ratio of 1:0.8. This is crucial evidence in the understanding of the oxidative route that TOPO takes as illustrated in the supporting material.

After the oxidation of TOPO at elevated temperatures and with an applied vacuum, DOPA, OPA and MOPA formation has been identified. The emergence of MOPA will be discussed below. First, DOPA was produced in the largest quantities as evidenced by the increase in the relative abundance of DOPA from 14% to 80% from pre and post-oxidation samples. DOPA formation should proceed by the oxidation of TOPO at the phosphorous atom by oxygen, the subsequent 1-octene leaving group and proton extraction from residual H_2O to acidify the molecule. Stoichiometric H_2O formation as a product of CdO/TDPA chelation was thoroughly analyzed by Liu *et al.* and Owen *et al.*, and found to reside in the reaction vessel.[43, 51] DOPA is traditionally synthesized in two routes: (1) utilizing 1-octene and hypophosphorous acid (H_2PO_2H) and (2) by oxidizing di-n-octylphosphine oxide (DOPO) in the presence of H_2O_2.[52, 53] Overall, the mechanistic details of such an oxidation step are very complex and beyond the scope of this present study. We believe that DOPA, in concert with OPA, is of direct importance to the anistropic growth of the CdSe QRs.

After a single alkyl chain was cleaved from the phosphorous atom in TOPO, DOPA was produced first and, as the oxidation continues, the second cleavage in turn produces OPA (Figure 5). OPA was produced in smaller quantities at a relative abundance of 8.7% after the oxidative step of the synthesis (Figure 4B). This is an order of magnitude increase over the pre-oxidation abundance of 0.75% that was detected prior to the oxidation step. This is a reasonable rate of turnover considering DOPA formation is a preceding step in the oxidative pathway toward OPA. In relative abundances, DOPA:OPA has a ratio of 1:0.109, and thus out

of approximately 10 available DOPA molecules, 1 OPA molecule is formed. Another molecule formed as a side product in the oxidation of TOPO is MOPA. MOPA was also detected by MS in negative polarity mode at 177.18 mass/charge units (SOM/S6). The relative abundance of MOPA was 1.9%, ca. 20% that of OPA. While MOPA was a minor product in the oxidative step, MOPA has been identified as aiding in the formation of high quality CdSe nanowires along with DOPA and OPA.[36]

^{31}P NMR spectroscopy was also utilized to look at the pre and post-oxidation solutions to detect any specific signatures of molecular TOPO and its derivatives (Figure 4A and B). The main peak present in the pre-combustion solution is that of TOPO at 49.2 ppm. Cd-TDPA which has been previously identified at ~25 ppm was not readily observed in our study.[49] Since concentration and molecular makeup of an individual sample can affect ^{31}P peak positions, we conclude that bound Cd-TDPA with TOPO could be lost under the TOPO peak. This discrepancy has not been fully determined. Control ^{31}P NMR studies of TDPA and chelated Cd-TDPA revealed peaks ranging from 25-35 ppm (SOM/S7). While DOPA was identified via MS prior to the oxidation of TOPO, ^{31}P NMR spectra were unable to readily resolve a representative peak. Post-oxidation solutions did reinforce the findings of the MS data and peaks representative of DOPA and OPA were found at 56.2 ppm and 32.5 ppm, respectively. As mentioned by Wang *et al*. previously, the relative peak shifting of TOPO and phosphinic/phosphonic acids are extremely sensitive to the other molecules present in solution and their relative amounts (Figure S17 of Ref. 36).[36, 44] Relative molecular ratios were not applied to the case of TOPO:DOPA or TOPO:OPA because of the relatively minute amounts observed. Pre and post-oxidation solutions did show a shift of 0.087 ppm in the ^{1}H NMR spectra representative of the protons on the alkyl chains of TOPO (SOM/S8). Overall, the use of MS was more sensitive with the resulting solutions, but we found it necessary to reinforce the presence of DOPA and OPA via an alternative experimental technique.

Historically, the organometallic method using TOPO for CdSe QD and QR synthesis is by far the most widespread, yet the decomposition of TOPO is rarely discussed. Previous investigation, in which only certain batches of technical TOPO of varied age produced QRs, was a good indication that phosphonic acids were responsible for anistropic growth. It is possible that the decomposed byproducts of aged TOPO produced over time in open air lab conditions were in fact DOPA, OPA and MOPA. While merely conjecture, long-term exposure of TOPO to O_2 and H_2O could result in the oxidation pathway that we highlighted, wherein successive alkyl chains are cleaved as a result of oxidation. In our case, this oxidative process took mere seconds to occur, as opposed to oxidation over a number of months in open air lab conditions. That being said, the long-term storage of TOPO in an inert atmosphere such as a glove box may be advantageous to reproducible synthesis sensitive to the presence of phosphinic/phosphonic acid byproducts.

Conclusion—Using commercially available high purity TOPO at elevated temperatures, in the presence of residual oxygen, and an applied vacuum, TOPO was decomposed to DOPA, OPA and MOPA. With DOPA and OPA in the reaction solvent mixture, CdSe QRs (~4 nm × 20 nm) were synthesized. This finding reinforces the work of Wang *et al*. in their systematic investigation of DOPA, OPA and MOPA addition and its influence on CdSe 1D nanostructure formation. In optically clear mixtures of Cd/TOPO/TDPA, the appearance of low concentration of DOPA had been detected prior to a high temperature vacuum application due to TOPO impurities, but did not produce QRs. Post-oxidation MS data revealed the added formation of additional DOPA, OPA and MOPA to the ligand-monomer solution. Subsequently, this lead to anistropic crystal growth along the 001 crystal axis of the CdSe nanocrystals and QR formation was observed. This chemical/morphological transformation only occurred in the presence of oxygen that was not removed due to a weak vacuum of <1000 mtorr during the degassing protocol. This study has demonstrated that in situ decomposition of TOPO into

DOPA, OPA and MOPA assists CdSe QR formation and the detailed ligand interaction is important to anistropic nanocrystal growth. Our findings suggest that oxidative products of aged TOPO could lead to the formation of a succession of phosphorous containing acids and thereby influence nanocrystal synthesis.

Supplementary Material

Refer to Web version on PubMed Central for supplementary material.

Acknowledgments

We would like to recognize funding support for the Mass Spectrometry Facility provided by the Thermo Electron Corporation (Seed funds), the W.M. Keck Foundation (Grant # 001768), and NIH's National Center for Research Resources (SIG # S10RR020939). AW would like to recognize funding through the Chancellor's Dissertation Year Fellowship at UCSC. The authors would like to thank the National Center for Electron Microscopy at Lawrence Berkeley National Laboratory for the use of its facilities. The author would especially like to thank Dr. Daniele Gerion and Dr. Natalia Zaitseva for guidance in the synthesis of quantum confined nanostructures. We are grateful to the Basic Energy Sciences Division of the US DOE (05ER4623A00) for financial support.

References

(1). Alivisatos AP, Harris TD, Brus LE, Jayaraman A. Journal of Chemical Physics 1988;89:5979.

(2). Bawendi MG, Carroll PJ, Wilson WL, Brus LE. Journal of Chemical Physics 1992;96:946.

(3). Bawendi MG, Wilson WL, Rothberg L, Carroll PJ, Jedju TM, Steigerwald ML, Brus LE. Physical Review Letters 1990;65:1623. [PubMed: 10042317]

(4). Brus L. Israel Journal of Chemistry 1993;33:9.

(5). Chestnoy N, Hull R, Brus LE. Journal of Chemical Physics 1986;85:2237.

(6). Marcus MA, Flood W, Stiegerwald M, Brus L, Bawendi M. Journal Of Physical Chemistry 1991;95:1572.

(7). Huynh WU, Dittmer JJ, Alivisatos AP. Science 2002;295:2425. [PubMed: 11923531]

(8). Manna L, Scher EC, Alivisatos AP. Journal Of The American Chemical Society 2000;122:12700.

(9). Ryan KM, Mastroianni A, Stancil KA, Liu HT, Alivisatos AP. Nano Letters 2006;6:1479. [PubMed: 16834433]

(10). Scher EC, Manna L, Alivisatos AP. Philosophical Transactions Of The Royal Society Of London Series A-Mathematical Physical And Engineering Sciences 2003;361:241.

(11). Manna L, Milliron DJ, Meisel A, Scher EC, Alivisatos AP. Nature Materials 2003;2:382.

(12). Hu JT, Ouyang M, Yang PD, Lieber CM. Nature 1999;399:48.

(13). Duan XF, Huang Y, Cui Y, Wang JF, Lieber CM. Nature 2001;409:66. [PubMed: 11343112]

(14). Gradecak S, Qian F, Li Y, Park HG, Lieber CM. Applied Physics Letters 2005;87

(15). Bruchez M, Moronne M, Gin P, Weiss S, Alivisatos AP. Science 1998;281:2013. [PubMed: 9748157]

(16). Gerion D, Pinaud F, Williams SC, Parak WJ, Zanchet D, Weiss S, Alivisatos AP. Journal Of Physical Chemistry B 2001;105:8861.

(17). Wolcott A, Gerion D, Visconte M, Sun J, Schwartzberg A, Chen SW, Zhang JZ. Journal Of Physical Chemistry B 2006;110:5779.

(18). Kim S, Lim YT, Soltesz EG, De Grand AM, Lee J, Nakayama A, Parker JA, Mihaljevic T, Laurence RG, Dor DM, Cohn LH, Bawendi MG, Frangioni JV. Nature Biotechnology 2004;22:93.

(19). Kazes M, Lewis DY, Ebenstein Y, Mokari T, Banin U. Advanced Materials 2002;14:317.

(20). Kamat PV. Journal Of Physical Chemistry C 2008;112:18737.

(21). Law M, Beard MC, Choi S, Luther JM, Hanna MC, Nozik AJ. Nano Letters 2008;8:3904. [PubMed: 18823149]

(22). Luther JM, Law M, Beard MC, Song Q, Reese MO, Ellingson RJ, Nozik AJ. Nano Letters 2008;8:3488. [PubMed: 18729414]

(23). Murray CB, Norris DJ, Bawendi MG. Journal Of The American Chemical Society 1993;115:8706.
(24). Peng XG, Wickham J, Alivisatos AP. Journal Of The American Chemical Society 1998;120:5343.
(25). Talapin DV, Rogach AL, Shevchenko EV, Kornowski A, Haase M, Weller H. Journal Of The American Chemical Society 2002;124:5782. [PubMed: 12010053]
(26). Manna L, Wang LW, Cingolani R, Alivisatos AP. Journal Of Physical Chemistry B 2005;109:6183.
(27). Zheng HM, Smith RK, Jun YW, Kisielowski C, Dahmen U, Alivisatos AP. Science 2009;324(5932): 1309–1312. [PubMed: 19498166]
(28). Bowers MJ, McBride JR, Rosenthal SJ. Journal Of The American Chemical Society 2005;127:15378. [PubMed: 16262395]
(29). Dagtepe P, Chikan V, Jasinski J, Leppert VJ. Journal Of Physical Chemistry C 2007;111:14977.
(30). Kudera S, Zanella M, Giannini C, Rizzo A, Li YQ, Gigli G, Cingolani R, Ciccarella G, Spahl W, Parak WJ, Manna L. Advanced Materials 2007;19:548.
(31). Riehle FS, Bienert R, Thomann R, Urban GA, Krugert M. Nano Letters 2009;9:514. [PubMed: 19140702]
(32). Huynh WU, Peng XG, Alivisatos AP. Advanced Materials 1999;11:923.
(33). Hu JT, Odom TW, Lieber CM. Accounts of Chemical Research 1999;32:435.
(34). Peng ZA, Peng XG. Journal Of The American Chemical Society 2001;123:1389.
(35). Peng ZA, Peng XG. Journal Of The American Chemical Society 2002;124:3343. [PubMed: 11916419]
(36). Wang F, Tang R, Kao JLF, Dingman SD, Buhro WE. Journal Of The American Chemical Society 2009;131:4983. [PubMed: 19296595]
(37). Manna L, Wang LW, Cingolani R, Alivisatos AP. Journal Of Physical Chemistry B 2005;109:6183.
(38). Puzder A, Williamson AJ, Zaitseva N, Galli G, Manna L, Alivisatos AP. Nano Letters 2004;4:2361.
(39). Rempel JY, Trout BL, Bawendi MG, Jensen KF. Journal of Physical Chemistry B 2005;109:19320.
(40). Rabani E. Journal of Chemical Physics 2001;115:1493.
(41). Milliron DJ, Hughes SM, Cui Y, Manna L, Li JB, Wang LW, Alivisatos AP. Nature 2004;430:190. [PubMed: 15241410]
(42). Becerra LR, Murray CB, Griffin RG, Bawendi MG. Journal of Chemical Physics 1994;100:3297.
(43). Liu HT, Owen JS, Alivisatos AP. Journal Of The American Chemical Society 2007;129:305. [PubMed: 17212409]
(44). Wang FD, Tang R, Buhro WE. Nano Letters 2008;8:3521. [PubMed: 18754691]
(45). Peng XG, Manna L, Yang WD, Wickham J, Scher E, Kadavanich A, Alivisatos AP. Nature 2000;404:59. [PubMed: 10716439]
(46). Kopping JT, Patten TE. Journal of the American Chemical Society 2008;130:5689. [PubMed: 18393427]
(47). Peng ZA, Peng XG. Journal of the American Chemical Society 2001;123:183. [PubMed: 11273619]
(48). Yu WW, Qu LH, Guo WZ, Peng XG. Chemistry Of Materials 2004;16:560.
(49). Wang W, Banerjee S, Jia SG, Steigerwald ML, Herman IP. Chemistry of Materials 2007;19:2573.
(50). Mokari T, Banin U. Chemistry Of Materials 2003;15:3955.
(51). Owen JS, Park J, Trudeau PE, Alivisatos AP. Journal Of The American Chemical Society 2008;130:12279. [PubMed: 18722426]
(52). Peppard DF, Mason GW, Lewey S. Journal of Inorganic Nuclear Chemistry 1965;27:2065.
(53). Williams RH, Hamilton LA. Journal Of The American Chemical Society 1952;74:5418.

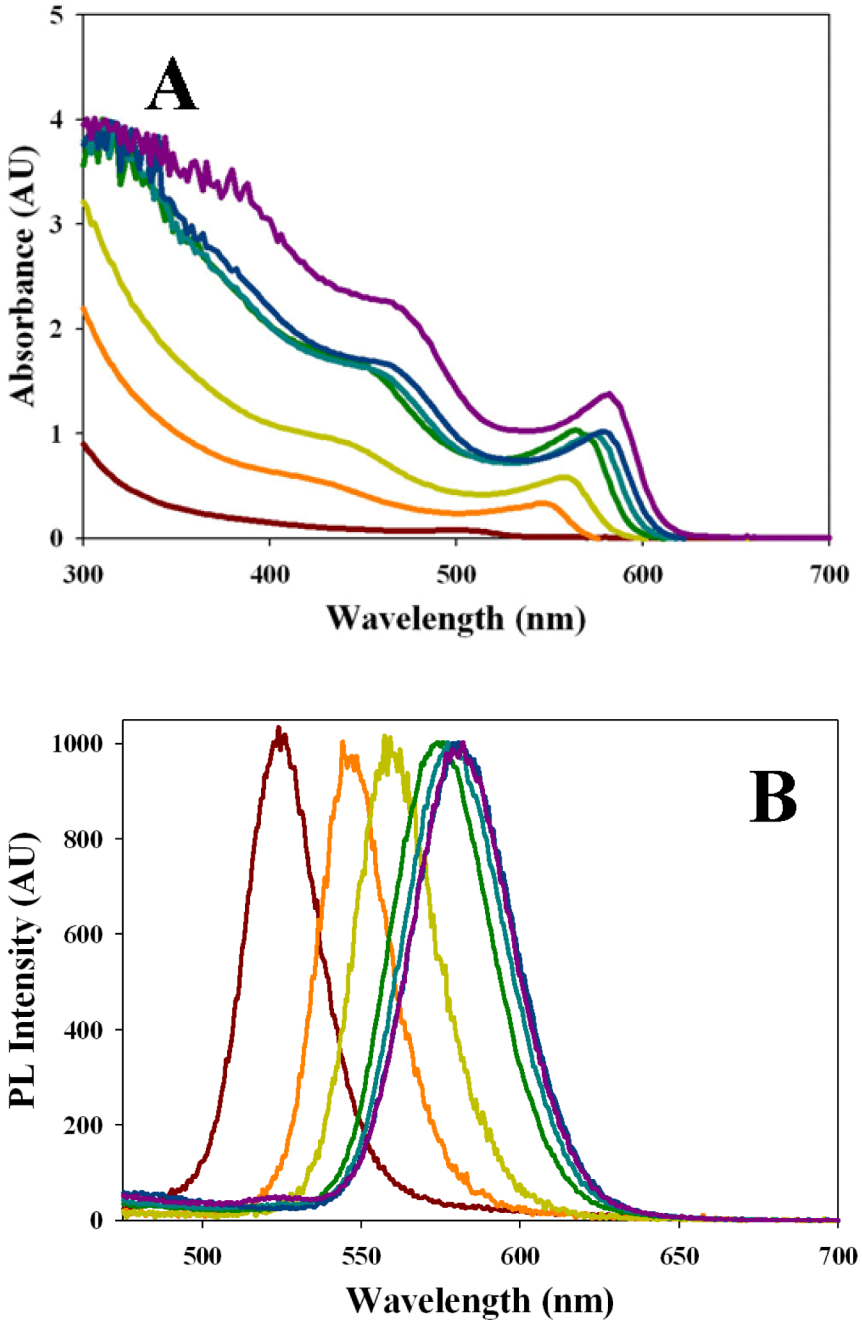

Figure 1.

UV-vis absorption spectra showing the growth of CdSe nanorods from 2 minutes to 20 minutes (**A**). Excitonic peak position red shifts as the inherent bandgap of the material becomes smaller in energy. PL spectra shows the consummate shifting of the bandedge emission as the CdSe nanorods are growing (**B**). The CdSe nanorods only display bandedge emission, and there are no apparent shallow or deep trap emissive states.

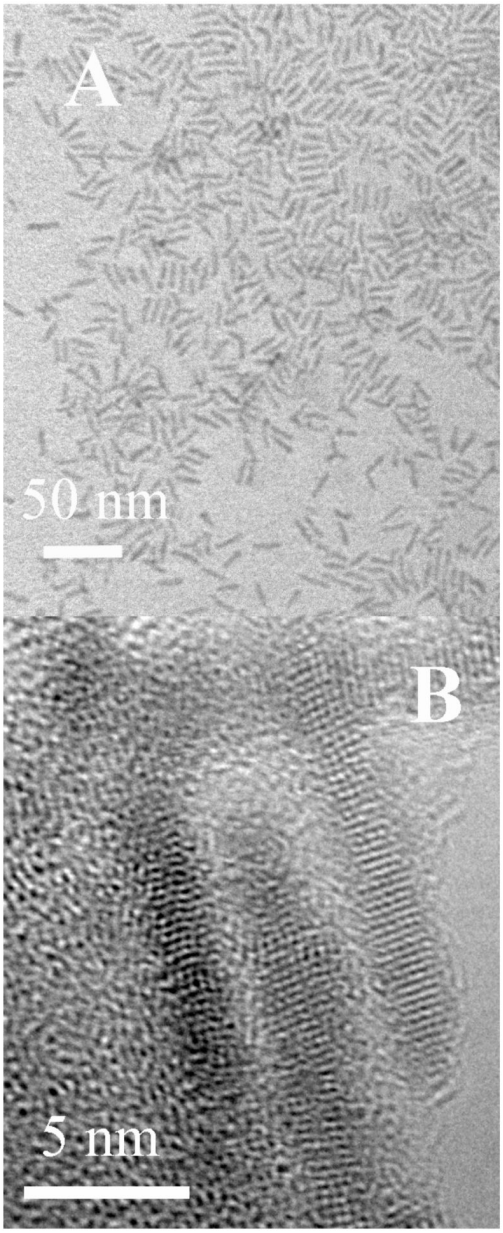

Figure 2.
TEM image of an ensemble of CdSe QRs with an approximate size of 4 nm × 20 nm (**A**). HRTEM image of three CdSe QRs reveal the crystal lattice of wurtzite CdSe. The lattice constant along the unique c-axis was found to be 3.57 Å, representative of the 001 crystal facet. Dislocations and vacancies can be observed in the length of the CdSe QRs (**B**).

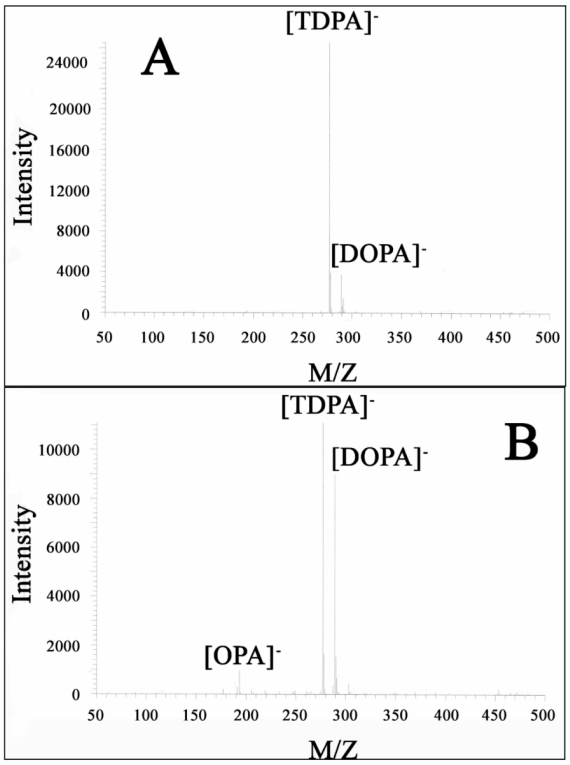

Figure 3.

MS data of solutions of Cd/TOPO/TDPA precursor solutions before (A) and after (B) combustion. The data was taken with a negative polarity and specifically probed the phosphonic acids within the precursor solution. Most notably is the appearance of a peak at 193 M/Z, representative of octylphosphonic acid (OPA). Other peaks of special interest are the dimers of OPA at 387.02 and the TDPA+OPA dimer at 471.05. Di-n-octylphosphinic acid (DOPA) is also found in the pre- and postcombustion solutions at 289.41, which consequently not show up in stock solutions of TDPA or TOPO.

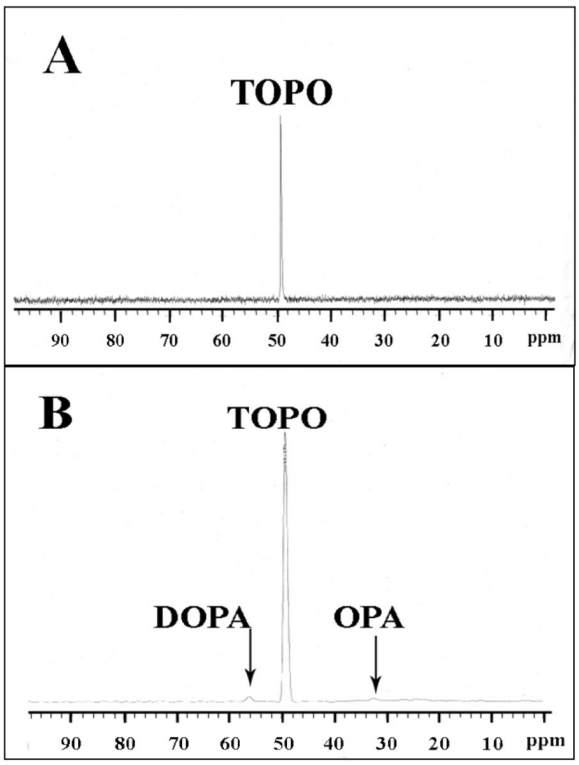

Figure 4.
^{31}P NMR spectra showing the presence of only TOPO prior to the oxidative step with a representative peak at ~49.2 ppm (**A**). After the oxidative step peaks emerge at 56.2 ppm and 32.5 ppm that have been identified as DOPA and OPA, respectively. Due to the relatively small amount of MOPA, it was not readily seen in the ^{31}P NMR spectra.

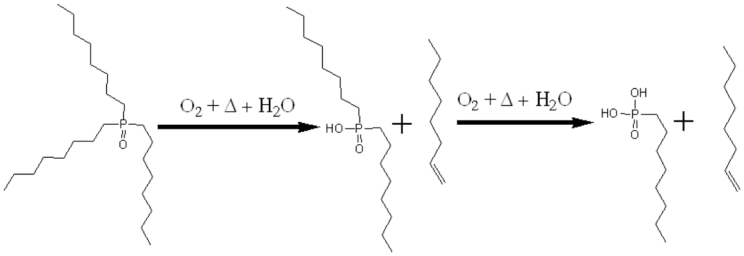

Figure 5.

Schematic representation of the oxidation of TOPO into three chemical species: (1) di-n-octylphosphonic acid (DOPA), (2) 1-octene, and (3) octylphosphonic acid (OPA). Mono-noctylphosphinic acid was left out for clarity. Specific oxidative mechanisms of TOPO are beyond the scope of the paper, but the general oxidative pathway is reinforced by both MS and NMR spectra. Strict stoichiometry was not enforced in this general mechanism.